Title
EXTL3 mutations cause skeletal dysplasia, immune deficiency, and developmental delay

Journal
Journal of Experimental Medicine, 214(3)

ISSN
0022-1007

Authors
Volpi, Stefano
Yamazaki, Yasuhiro
Brauer, Patrick M
et al.

Publication Date
2017-03-06

DOI
10.1084/jem.20161525

Peer reviewed

EXTL3 mutations cause skeletal dysplasia, immune deficiency, and developmental delay

Stefano Volpi,[1] Yasuhiro Yamazaki,[3] Patrick M. Brauer,[5] Ellen van Rooijen,[6] Atsuko Hayashida,[7] Anne Slavotinek,[10] Hye Sun Kuehn,[4] Maja Di Rocco,[2] Carlo Rivolta,[12] Ileana Bortolomai,[14,22] Likun Du,[8] Kerstin Felgentreff,[8] Lisa Ott de Bruin,[8] Kazutaka Hayashida,[7] George Freedman,[11] Genni Enza Marcovecchio,[14] Kelly Capuder,[8] Prisni Rath,[15] Nicole Luche,[8] Elliott J. Hagedorn,[6] Antonella Buoncompagni,[1] Beryl Royer-Bertrand,[12,13] Silvia Giliani,[16] Pietro Luigi Poliani,[17] Luisa Imberti,[18] Kerry Dobbs,[3] Fabienne E. Poulain,[19] Alberto Martini,[1] John Manis,[9] Robert J. Linhardt,[20] Marita Bosticardo,[14] Sergio Damian Rosenzweig,[4] Hane Lee,[21] Jennifer M. Puck,[11] Juan Carlos Zúñiga-Pflücker,[5] Leonard Zon,[6] Pyong Woo Park,[7] Andrea Superti-Furga,[13] and Luigi D. Notarangelo[3]

[1]Unita' Operativa Pediatria 2 and [2]Unit of Rare Diseases, Department of Pediatrics, Istituto Giannina Gaslini, 16148 Genoa, Italy
[3]Laboratory of Host Defenses, National Institute of Allergy and Infectious Diseases and [4]Department of Laboratory Medicine, National Institutes of Health Clinical Center, National Institutes of Health, Bethesda, MD, 20892
[5]Department of Immunology, Sunnybrook Research Institute, University of Toronto, Toronto, Ontario M5S, Canada
[6]Stem Cell Program, [7]Division of Respiratory Diseases, [8]Division of Immunology, and [9]Department of Laboratory Medicine, Boston Children's Hospital, Harvard Medical School, Boston, MA 02115
[10]Department of Pediatrics, Division of Genetics and [11]Department of Pediatrics, University of California, San Francisco, San Francisco, CA 94143
[12]Department of Computational Biology, Unit of Medical Genetics and [13]Division of Genetic Medicine, Lausanne University Hospital, University of Lausanne, 1015 Lausanne, Switzerland
[14]San Raffaele Telethon Institute for Gene Therapy, Istituto di Ricerca e Cura a Carattere Scientifico San Raffaele Scientific Institute, 20132 Milan, Italy
[15]Tata Consultancy Services Innovation Labs, Telangana 500081, India
[16]A. Nocivelli Institute for Molecular Medicine and [17]Department of Molecular and Translational Medicine, University of Brescia, 25123 Brescia, Italy
[18]Centro di ricerca emato-oncologica AIL, Spedali Civili, 25123 Brescia, Italy
[19]Department of Biological Sciences, University of South Carolina, Columbia, SC 29208
[20]Department of Chemistry and Chemical Biology, Rensselaer Polytechnic Institute, Troy, NY 12180
[21]Department of Pathology and Laboratory Medicine, University of California at Los Angeles, Los Angeles, CA 90095
[22]Consiglio Nazionale delle Ricerche–Istituto di Ricerca Genetica e Biomedica, Milan Unit, 20138 Milan, Italy

We studied three patients with severe skeletal dysplasia, T cell immunodeficiency, and developmental delay. Whole-exome sequencing revealed homozygous missense mutations affecting exostosin-like 3 (EXTL3), a glycosyltransferase involved in heparan sulfate (HS) biosynthesis. Patient-derived fibroblasts showed abnormal HS composition and altered fibroblast growth factor 2 signaling, which was rescued by overexpression of wild-type *EXTL3* cDNA. Interleukin-2–mediated STAT5 phosphorylation in patients' lymphocytes was markedly reduced. Interbreeding of the *extl3*-mutant zebrafish (*box*) with Tg(*rag2:green fluorescent protein*) transgenic zebrafish revealed defective thymopoiesis, which was rescued by injection of wild-type human *EXTL3* RNA. Targeted differentiation of patient-derived induced pluripotent stem cells showed a reduced expansion of lymphohematopoietic progenitor cells and defects of thymic epithelial progenitor cell differentiation. These data identify *EXTL3* mutations as a novel cause of severe immune deficiency with skeletal dysplasia and developmental delay and underline a crucial role of HS in thymopoiesis and skeletal and brain development.

INTRODUCTION

Heparan sulfate (HS) is a sulfated linear polysaccharide consisting of repeating disaccharide units of either glucuronic or iduronic acid, alternating with *N*-acetyl-glucosamine. HS is heterogeneously sulfated at the *N*, 6-*O*, and 3-*O* positions of glucosamine and at the 2-*O* position of uronic acids. All HS in vivo is found covalently bound to specific core proteins as HS proteoglycans (HSPGs; Reichsman et al., 1996; Stewart and Sanderson, 2014; Ortmann et al., 2015). HSPGs bind to and regulate the activity of morphogens that provide timed

Correspondence to Luigi D. Notarangelo: luigi.notarangelo2@nih.gov; or Andrea Superti-Furga: asuperti@unil.ch

Abbreviations used: 3D, three-dimensional; CK, cytokeratin; DE, definitive endoderm; ERK, extracellular signal–regulated kinase; EXT, exostosin; EXTL3, EXT-like 3; FGF, fibroblast growth factor; FGFR, FGF receptor; HPC, hematopoietic progenitor cell; HS, heparan sulfate; HSPG, HS proteoglycan; iPSC, induced pluripotent stem cell; KSR, knockout serum replacement; LV, lentivirus; MACS, magnetic-activated cell sorting; MEF, mouse embryonic fibroblast; TBP, TATA-binding protein; TEC, thymic epithelial cell; TEP, thymic epithelial progenitor; TREC, TCR excision circle; WES, whole-exome sequencing.

The Rockefeller University Press $30.00
J. Exp. Med. 2017 Vol. 214 No. 3 623–637
https://doi.org/10.1084/jem.20161525

The Journal of Experimental Medicine

and spatially regulated developmental cues that control skeletal patterning (Revest et al., 2001a), thymus organogenesis (Rodewald, 2008), thymic epithelial cell (TEC) differentiation (Dooley et al., 2007; Saldaña et al., 2016), and lymphopoiesis (Borghesi et al., 1999).

The exostosin (EXT) family of genes encodes glycosyltransferases involved in the initiation of HS biosynthesis and elongation of HS chains (Esko and Lindahl, 2001; Busse et al., 2007). Conditional deletion of the *Ext1* gene from limb mesenchyme causes skeletal defects with shortening of long bones in mice (Matsumoto et al., 2010), and both *dak* and *box* zebrafish (with mutations in the *ext2* and in the EXT-like 3 [*extl3*] genes, respectively) show defects of pectoral fin and branchial arch development (Schilling et al., 1996; van Eeden et al., 1996; Norton et al., 2005).

Primary immunodeficiencies include over 300 distinct disorders (Picard et al., 2015), and genetic disorders of the skeleton include over 450 disorders (Bonafe et al., 2015). A small number of disorders exist that combine a skeletal dysplasia with immune dysfunction of variable severity. Among these, the best-defined entities are cartilage-hair hypoplasia, Schimke immuno-osseous dysplasia, and spondyloenchondromatosis, but other conditions have been described (Gatti et al., 1969; MacDermot et al., 1991; Schofer et al., 1991; Corder et al., 1995; Castriota-Scanderbeg et al., 1997; Clewing et al., 2007) whose molecular bases have remained elusive so far.

Here, we report biallelic *EXTL3* mutations in three patients from two families with severe T cell immunodeficiency, skeletal dysplasia, and neurodevelopmental delay and provide evidence for a critical role of HS in human thymopoiesis and skeletal development.

RESULTS AND DISCUSSION

Clinical phenotype and imaging studies

We studied three patients from two families who presented at birth with short-limb skeletal dysplasia and severe T cell immunodeficiency (Fig. 1 and the Case studies section of Materials and methods). Skeletal radiography revealed similar abnormalities at birth in all three patients (Fig.1, D–L) consisting of: generalized platyspondyly with increased intervertebral space, narrow sacro-ischiatic notches with trident-shaped acetabula, and short and plump limb bones, metacarpals, and phalanges. Premature craniosynostosis was seen in the skull x ray and computed tomography studies of patient 1 (P1) and P2, with cloverleaf deformity in P2. All three patients had narrowing of the cervical canal, and severe narrowing of the laryngotracheal tract was present in P1 and P2. Neurological abnormalities included: opisthotonus, hyperreflexia, generalized seizures, and developmental delay in P1; clonic arm movements, nystagmus, and developmental arrest in P2; and muscular hypotonia and marked developmental delay in P3.

Immunological studies

P2 and P3 manifested in the first month of life a T^- B^+ NK^+ SCID phenotype, which in P3 was ascertained after positive newborn screening for SCID (Fig. 1 M). The presence of autologous, activated, and oligoclonal T cells, associated with generalized exfoliative dermatitis suggestive of Omenn syndrome, was documented in P1 (Fig. 1 A). Impaired proliferation to mitogens and eosinophilia was documented in all three infants. Hypogammaglobulinemia but increased IgE serum levels were detected in P1 and P2. At 1 yr and 4 mo of age, partial recovery of T cell count and function was documented in P3, who has mounted antibody responses to killed and live vaccines.

Genetic analysis

As the radiographical findings at birth were reminiscent of fibroblast growth factor (FGF) receptor 3 (FGFR3)–associated dysplasias and craniosynostosis and laryngeal narrowing are associated with *FGFR1* and *FGFR2* mutations (Hockstein et al., 2004), we sequenced *FGFR1*, *FGFR2*, and *FGFR3* genes, but no mutations were identified. The notion that the parents of P1 and P2 were from the same village, together with the rarity of the condition, led us to assume autosomal recessive inheritance with consanguinity by descent as a probable genetic basis of the disease in family 1. Whole-exome sequencing (WES) revealed three small regions of homozygosity on chromosomes 4, 6, and 8 in P1 and P2 but not in their parents. Upon filtering (Fig. S1), only four genes (*FCGBP*, *HEATR5A*, *MICAL3*, and *EXTL3*) carried variants that were compatible with mutations causing a rare, recessively inherited disease in this family (Tables S1 and S2). WES was also performed in P3 and in her parents. Upon filtering (Fig. S1), one de novo heterozygous variant, four homozygous variants, and eight compound heterozygous variants in four genes were detected in P3 (Tables S1 and S2).

EXTL3 was the only gene in which biallelic variants were identified in P1 and P2 (c.1015C>T; p.R339W), as well as in P3 (c.1382C>T; p.P461L; Fig. 1 N), whereas the respective parents were heterozygous for the same mutations. The identification of mutations in the same gene in both families sharing a similar phenotype makes *EXTL3* a strong candidate gene. To further support this hypothesis: (a) the p.R339W variant is not reported in public or private databases, and the p.P461L variant is reported at very low frequency in Exome Aggregation Consortium database (Tables S1 and S2); (b) both mutations affect highly conserved residues (Fig. 1 O) and are predicted to be deleterious by Polyphen2, pMUT, Sorting Intolerant From Tolerant (SIFT), Mutation taster, Synonymous Non-synonymous Analysis Program (SNAP), SNP, and Gene Ontology databases; (c) their combined annotation-dependent depletion Phred score (17.64 for the p.R339W mutation and 15.4 for the p.P461L mutation) is significantly higher than the mutation significance cut off (Itan et al., 2016), which for the *EXTL3* gene is 8.931; and (d) defects of skeletal development had been previously reported in the box^{tm70g} zebrafish carrying a hypomorphic (D831N) *extl3* mutation (Schilling et al., 1996; van Eeden et al., 1996; Lee et al., 2004).

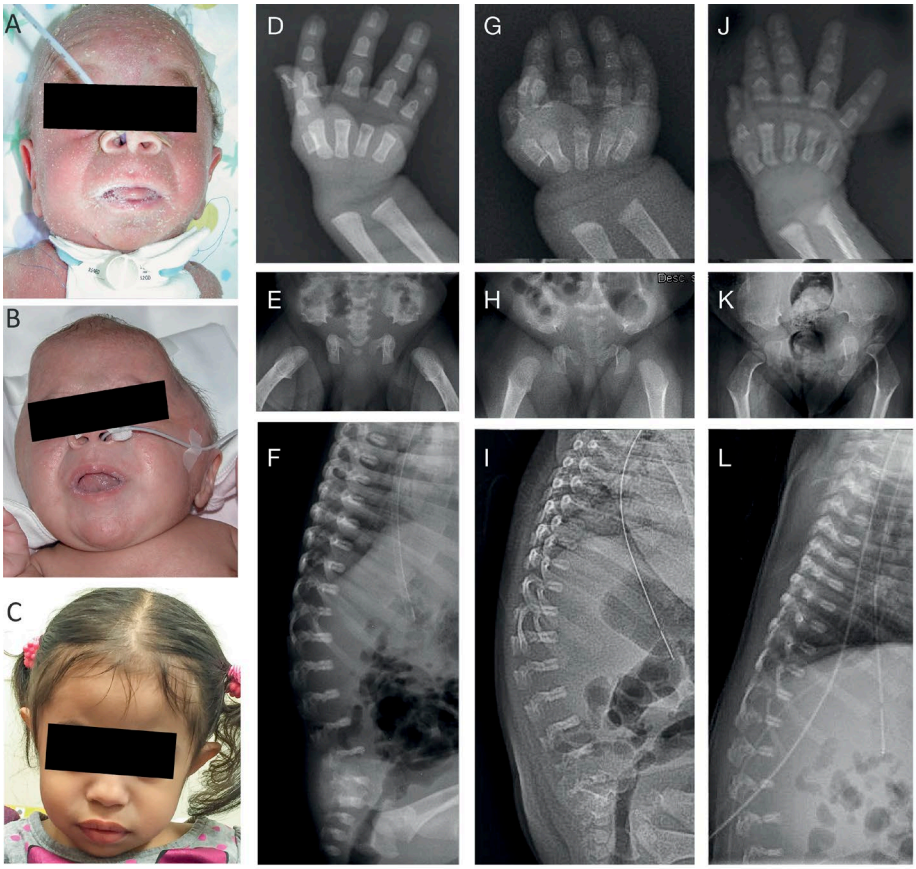

M

	P1 (3 mo)	P2 (3 mo)	P3 (1 mo)	Reference values
ALC (cells/μL)	2100	1500	1800	3900-9000
Eosinophils (cells/μL)	1200	700	1500	50-420
CD3 (cells/μL)	1105	81	196	2560-5600
CD4 (cells/μL)	1042	76	160	1800-4000
naive CD4 (% of $CD4^+$)	<1	n.d.	40	64-92
memory CD4 (% of $CD4^+$)	99.4	n.d.	49	3-16
CD8 (cells/μL)	40	3	36	590-1600
CD19 (cells/μL)	531	1275	1206	430-3000
$CD3^-$ $CD56^+$ (cells/μL)	346	133	198	170-830
IgG (mg/dl)	62	152	733[a]	164-588
IgA (mg/dl)	<4	9	16	16-50
IgM (mg/dl)	34	55	40	32-132
IgE (kU/L)	>2000	1675	27	1-30
In vitro response to PHA	1.2[b]	no mitoses[c]	22[d]	27.8-280.7[b]; ≥50[d]

[a] of maternal origin; [b] cpm $x10^{-3}$; [c] at karyotype examination; [d] % of $CD45^+$ cells dividing

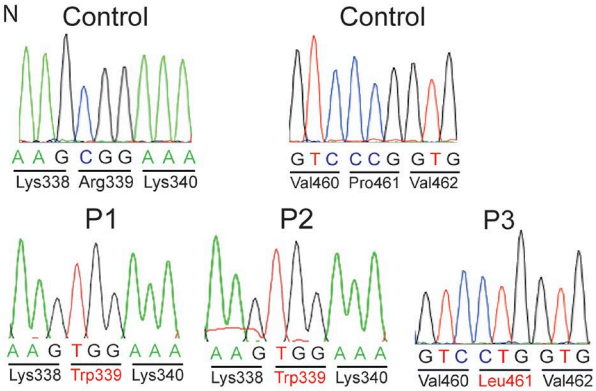

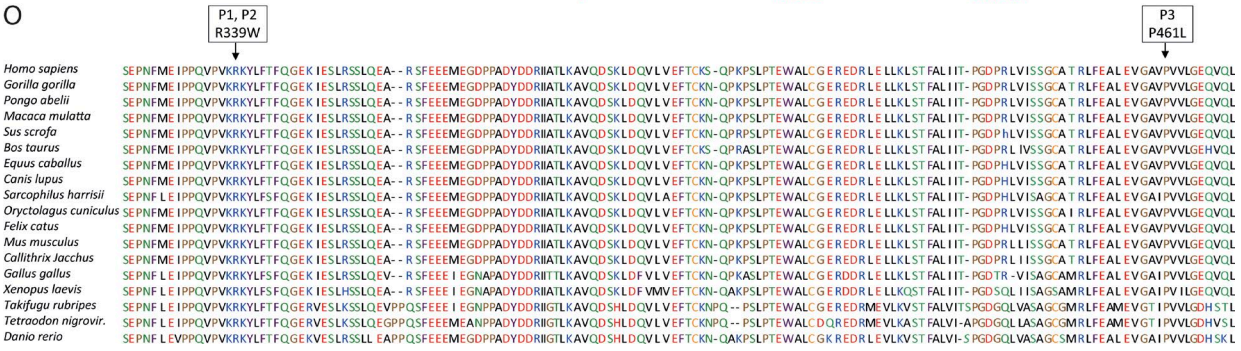

Figure 1. **Clinical and immunological phenotype and mutation analysis.** (A–C) Clinical image of P1 (showing exfoliative erythroderma) at 9 mo of age (A), cloverleaf skull and bulging fontanelle in P2 at age 2 mo (B), and P3 at age 2 yr and 6 mo showing a moderately bulging forehead and sunken nasal

The EXTL3 R339W mutation causes abnormalities of HS production

Western blotting showed similar levels of EXTL3 protein expression in fibroblasts from P1 and a healthy control and in PBMCs from P3 and a healthy donor (Fig. 2 A). P1- and control-derived fibroblasts produced equivalent amount of HS (0.131 and 0.117 μg/10^6 cells, respectively). However, longer HS chains in the patient sample were detected by Alcian blue staining of HS extracted from EBV-transformed B cells and fractionated by 5–12% gradient SDS-PAGE (Fig. 2 B). Furthermore, extracted ion chromatogram liquid chromatography–mass spectrometry revealed an abnormal HS sulfation pattern in P1's fibroblasts, with increase in 6-*O*–sulfated and 2-*O*–sulfated disaccharides, which was corrected by EXTL3 overexpression upon transduction of P1's fibroblasts with a lentiviral vector encoding for a wild-type copy of *EXTL3* cDNA (Fig. 2, A and C). Increase in 6-*O*–sulfated disaccharides and longer HS chains have been previously demonstrated upon siRNA-mediated silencing of *EXTL3* in HEK-293 (Busse et al., 2007). Altogether, these results indicate that the EXTL3 R339W mutation is a hypomorphic allele that alters the function of the enzyme and leads to longer HS chains with an aberrant sulfation pattern.

Abnormalities of intracellular signaling in EXTL3-mutated cells

All three patients presented clinical and radiographical features that were reminiscent of those associated with *FGFR* mutations causing increased intracellular signaling (Tavormina et al., 1995). Longer HS chains containing an increased amount of 6-*O* sulfates have been previously shown to provide an additional binding site for FGFR, increasing FGF signaling (Sugaya et al., 2008; El Masri et al., 2016). As compared with control-derived fibroblasts, P1's cells showed increased extracellular signal–regulated kinase (ERK) phosphorylation upon FGF2 stimulation, and this abnormality was corrected by overexpression of wild-type EXTL3 (Fig. 2 D). These results indicate that by altering HS chain length and composition, *EXTL3* mutations potentiate FGF2 signaling, thereby contributing to the pathophysiology of the skeletal dysplasia observed in the patients.

HS plays an important role also in regulating signaling in response to various cytokines, including IL-2 (Wrenshall et al., 2003) and IL-7 (Milne et al., 2008). Upon stimulation of PBMCs from P3 and a healthy control with various cytokines, we observed marked reduction of STAT5 phosphorylation in P3's PBMCs in response to IL-2, with a more subtle defect in response to IL-7 (Fig. 2 E).

extl3-mutant zebrafish have defective thymopoiesis

Abnormalities of cartilage development and defective pectoral fin formation had been previously reported in *extl3*-mutant zebrafish (*box*; Schilling et al., 1996; van Eeden et al., 1996; Lee et al., 2004; Norton et al., 2005) and confirmed by us (Fig. 3 A), but no information was available on thymic development in the mutant fish. To investigate this, we crossed *extl3/box* zebrafish with *Tg(rag2:gfp)* transgenic zebrafish (Jessen et al., 2001) and analyzed expression of the GFP to visualize the thymus in developing embryos (Langenau et al., 2004). In-vivo immunofluorescence analysis revealed a decreased GFP signal in mutant animals compared with siblings (Fig. 3 B), and confocal imaging followed by isosurface three-dimensional (3D) reconstruction demonstrated a 50% decrease in the volume occupied by GFP^+ cells (Fig. 3, C and D). To prove that the defect is caused by the *extl3* mutation, we injected mutant and sibling zygotes with wild-type human *EXTL3* mRNA and observed rescue of the thymic phenotype (Fig. 3 E). Normalization of pectoral fin development was also achieved (Fig. 3 E), as previously reported, with injection of wild-type zebrafish *extl3* mRNA (Lee et al., 2004). The EXTL3 protein may also serve as a receptor for the regenerating (REG) protein family, functioning independently from HS production (Levetan et al., 2008; Acquatella-Tran Van Ba et al., 2012; Lai et al., 2012). To dissect which of these two functions of EXTL3 has a role in thymocyte development, we studied the dak^{to273}-mutant zebrafish, which carries a null mutation in *ext2*, associated with severe reduction in HS production (Lee et al., 2004) and abnormalities of fin and branchial arch development (Fig. 3 F). *EXT2* is involved in HS biosynthesis (McCormick et al., 2000; Senay et al., 2000) but has no known role in REG protein signaling. A marked decrease of thymus volume was also observed in *ext2/dak* Tg*(rag2:gfp)* zebrafish (Fig. 5, G and H), providing definitive evidence in vivo that HS plays an important role in thymopoiesis.

Patient-derived induced pluripotent stem cell (iPSCs) have reduced ability to generate lymphoid progenitor cells and to differentiate to thymic epithelial progenitor (TEP) cells

HS modulates the activity of morphogens and growth factors involved in mesodermal and hematopoietic progenitor cell (HPC) differentiation (Holley et al., 2011; Kraushaar et al., 2012) and in expansion and maturation of lymphoid progenitor cells (Borghesi et al., 1999). To gain insights into the pathophysiology of impaired T cell development in patients with EXTL3 deficiency, we generated iPSCs from

root with full cheeks (C). (D–L) Radiographs show short metacarpals and phalanges, open iliac wings, narrow sacro-ischiatic notches, radiolucent band at proximal femurs reminiscent of achondroplasia, and severe diffuse platyspondyly with expanded intervertebral spaces. In the pelvis of P3, there is coxa valga with delayed ossification of femoral heads, acetabular dysplasia, and hip subluxation. (D–F) P1; (G–I) P2; (J–L) P3. All radiographs were taken at birth, except for the pelvis of P3 (K), which was taken at 2 yr and 5 mo. (M) Laboratory data at diagnosis. ALC, absolute lymphocyte count. (N) Chromatograms demonstrating homozygosity for *EXTL3* mutations in the affected patients. (O) Evolutionary conservation of the EXTL3 protein in the region containing the mutations detected in patients.

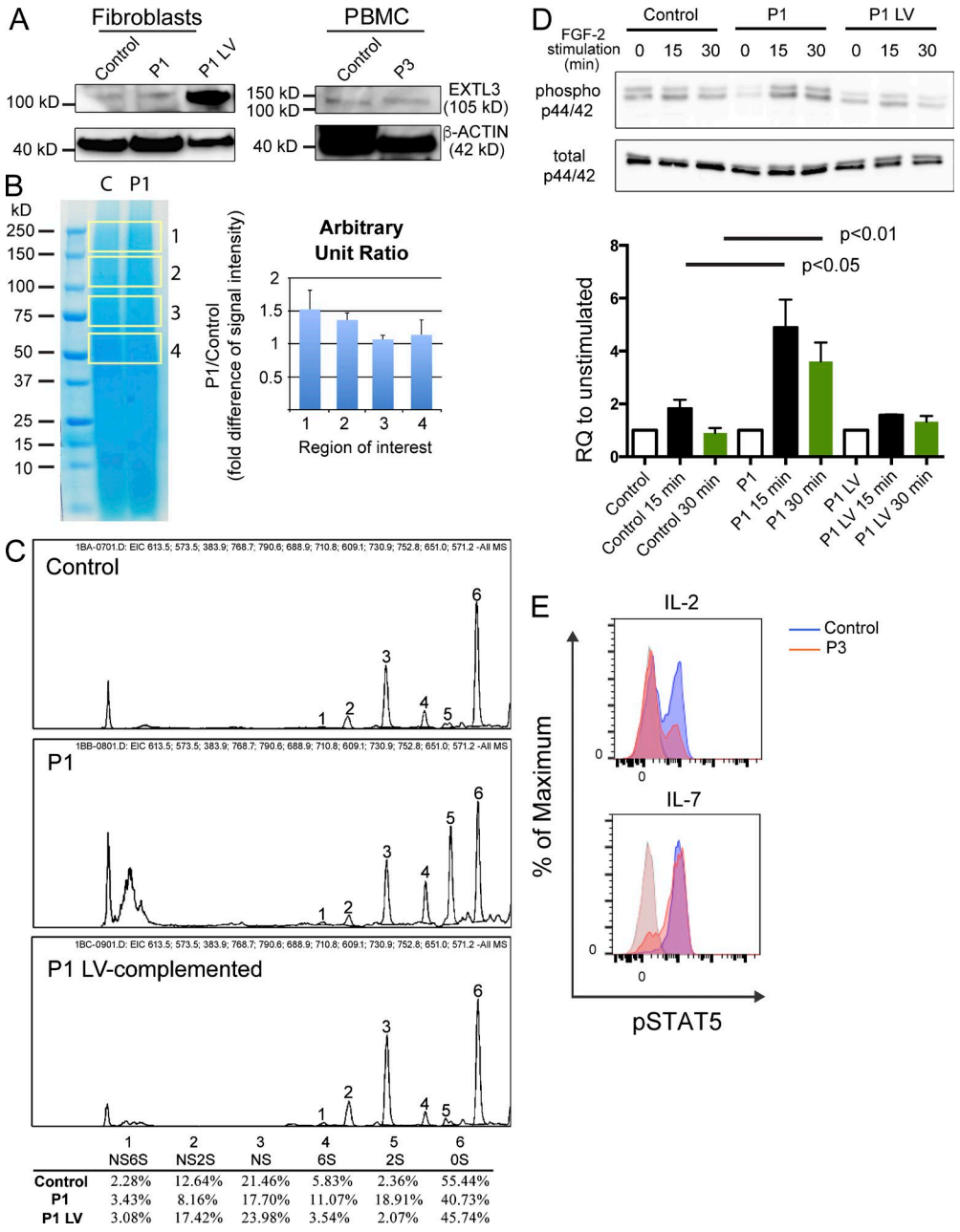

	1 NS6S	2 NS2S	3 NS	4 6S	5 2S	6 0S
Control	2.28%	12.64%	21.46%	5.83%	2.36%	55.44%
P1	3.43%	8.16%	17.70%	11.07%	18.91%	40.73%
P1 LV	3.08%	17.42%	23.98%	3.54%	2.07%	45.74%

Figure 2. ***EXTL3* mutations affect HS composition and cell signaling.** (A, left) Western blot analysis of EXTL3 protein expression in fibroblasts from a control and P1 and in P1's fibroblasts complemented with a lentiviral vector–expressing wild-type *EXTL3* (P1 LV). (Right) Western blot analysis of EXTL3 protein expression in PBMCs from a control and P3. β-actin was used as a loading control. Shown is a representative image of $n = 3$ experiments. (B, left) Alcian blue staining of HS length in EBV-B cell lines from control (C) and P1, as assessed by 5–12% SDS-PAGE. (Right) Relative quantification of content of HS's of various length (defined by regions of interest; boxes on the left) in P1 versus control. Shown is the mean ± SD from one representative experiment of two. (C) Disaccharide composition analysis of HS chains, showing an increase in 6-*O*-sulfated and 2-*O*-sulfated disaccharides (peaks 4 and 5) in P1 cells, which was corrected by complementation with P1 LV. Shown are representative images of $n = 2$ experiments. (D, top) Western blot analysis of ERK phosphorylation (p44/42) at 0, 15, and 30 min after FGF2 stimulation of control, P1, and P1 LV fibroblasts. Shown is a representative image from three (P1 LV) and five (control and P1) replicates. (Bottom) Relative quantification (RQ) of the ratio between phospho-p44/42 and total p44/42 signal in stimulated versus unstimulated conditions. Shown is the mean ± SD from the same experiments as in the top panel. Statistical significance was assessed with two-tail Student's *t* tests. (E) Overlays of flow cytometry histograms of phospho-STAT5 (pSTAT5) signal in unstimulated (tinted) and cytokine-stimulated (solid) PBMCs from a healthy control and P3. Gating was on $CD4^+$ cells. Shown is one representative experiment of two.

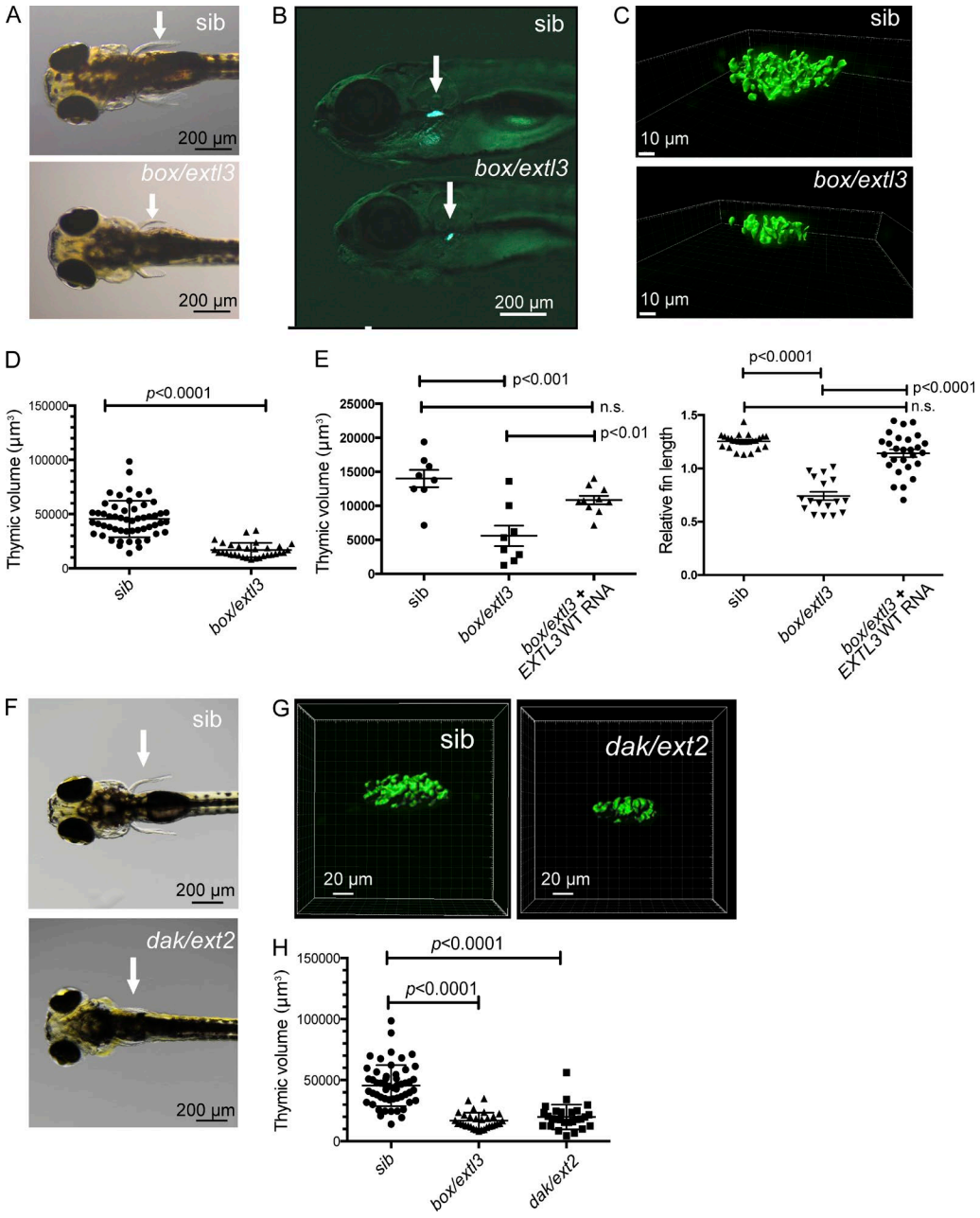

Figure 3. ***extl3/box*-mutant zebrafish has defective thymopoiesis that is rescued by injection of *EXTL3* wild-type RNA.** (A) *Extl3/box*-mutant fish have shorter pectoral fins (arrows). (B) Immunofluorescence image of *RAG2-GFP* expression in 6-d postinfection (dpf) *extl3/box Tg*(*rag2:gfp*) larvae. Arrows indicate the thymus. (C and D) Representative images of isosurface 3D reconstruction (C) and total volume quantification (D) of thymic GFP signal from 6-dpf *extl3/box Tg*(*rag2:gfp*) larvae. (A–D) Shown are representative data of >50 sibling (sib) and 30 *box* animals from three independent experiments. (E) Rescue of thymic volume (left) and pectoral fin length (right) in 6-dpf *extl3/box Tg*(*rag2:gfp*) larvae injected with 100 ng *EXTL3* wild-type RNA. Relative fin length indicates the ratio between lengths of fin to eye. $n = 2$ experiments. Error bars represent SEM. (F) *Ext2/dak*-mutant fish have shorter pectoral fins. (G and H) Representative images of isosurface 3D reconstruction (G) and total volume quantification (H) of thymic GFP signal from 6-dpf *ext2/dak Tg*(*rag2:gfp*) larvae. (F–H) Shown are representative images of >50 sibling, 30 *box*, and 27 *dak* animals from three independent experiments. Statistical significance was assessed using two-tail unpaired Student's *t* test (D) and one-way ANOVA with Bonferroni post-analysis (E and H).

P1 and from a healthy control (Fig. 4, A–C) and differentiated them toward HPCs and T lymphocytes (Brauer et al., 2016). Patient-derived iPSCs manifested a defect in embryoid body size and cell number and exhibited impaired expansion of HPCs (Fig. 4 D). A similar phenotype was previously reported during in vitro differentiation of *Ext1*$^{-/-}$ mouse

embryonic stem cells to embryoid bodies and hemangioblasts (Holley et al., 2011; Kraushaar et al., 2012). Upon co-culture on OP9-DL4 stromal cells, expansion of EXTL3-deficient cells was greatly diminished (Fig. 4 E); however, expression of markers indicative of T cell lineage commitment and maturation was preserved (Fig. 4 F). These data indicate that EXTL3 plays a critical role in the expansion of HPCs but may not be required at later stages of T cell differentiation, although a possible compensatory role of HS provided in trans by the OP9-DL4 cells in this system cannot be excluded.

By modulating FGF signaling, HSPG also regulates the differentiation and proliferation of TECs (Anderson and Jenkinson, 2001; Revest et al., 2001b; Rodewald, 2008). In the human thymus, TECs express EXTL3 at higher levels than hematopoietic cells (Fig. 5 A). To address whether *EXTL3* mutations affect TEC differentiation, we applied to human iPSCs a protocol used to induce differentiation of human embryonic stem cells to definitive endoderm (DE), ventral pharyngeal endoderm, and TEP cells (Parent et al., 2013). Timely regulated exposure to a defined set of developmental cues (Fig. 5 B) allowed progressive differentiation of control-derived iPSCs, with differential expression of genes that mark DE, ventral pharyngeal endoderm, and TEP stages (Fig. 5 C). At the end of the culture, confocal microscopy demonstrated coexpression of cytokeratin 8 (CK8) and CK5 and nuclear expression of FOXN1 (Fig. 5 D), confirming the TEP phenotype (Parent et al., 2013; Sun et al., 2013; Su et al., 2015). Comparative analysis of gene expression by quantitative PCR at the TEP stage demonstrated that EXTL3-mutated cells had decreased expression of *TBX1*, *EYA1*, and *CK5*, as compared with control-derived cells, and a similar trend was observed for *FOXN1* (Fig. 5 E). In contrast, EXTL3-mutated cells retained high levels of *SOX17* expression, which in control cells reaches a peak of expression at the DE stage and is then down-regulated. Altogether, these data indicate that EXTL3 deficiency also affects TEC differentiation.

In summary, our results show that *EXTL3* mutations in humans cause abnormalities of HS length and composition that alter cellular responses and result in T cell immunodeficiency, skeletal dysplasia, and neurological complications. Future studies may clarify whether the spontaneous improvement of T cell count in P3 is part of the natural history of the disease or expression of a milder phenotype. Finally, this study expands the number of SCID-related disorders that can be identified with newborn screening.

MATERIALS AND METHODS

Case studies

P1 and P2 were siblings born to parents of North African descent from the same village of Tunisia. The older patient (P1) was born at term by C-section because of severe fetal distress. P1's weight was 2,315 kg (less than third percentile), length was 48 cm (10th percentile), and head circumference was 35 cm (50th percentile). Short limbs and scaphocephaly were apparent. Mechanical ventilation was necessary because of respiratory distress. Laryngotracheal narrowing was found on laryngeal endoscopy, abdominal sonography revealed the presence of multiple liver cysts, and craniocervical magnetic resonance imaging showed impingement of the posterior arch of C1 on the medulla with mild stenosis of the cervical canal requiring neurosurgery. Over the first months of life, short-limbed dwarfism (length at age 4 mo less than third percentile) became evident. The patient developed *Klebsiella* and *Staphylococcus aureus* sepsis at 3 mo and generalized exfoliating dermatitis at 5 mo (Fig. 1 A). Immunological evaluation at that time demonstrated that >97% of circulating $CD4^+$ and $CD8^+$ cells had an activated/memory ($CD45RA^-$) phenotype. Maternal T cell engraftment was ruled out by microsatellite analysis, and oligoclonality of circulating T cells was demonstrated by heteroduplex analysis of T cell receptor β variable (*TCRBV*) gene rearrangement PCR products. TCR excision circles (TRECs) at that time were undetectable (normal value: >41/μl). Neurological abnormalities included opisthotonus with generalized hyperreflexia, generalized seizures, and absence of any interaction with the environment. The infant deceased at 11 mo of age after a history of recurrent infections.

A younger sister (P2) was born at gestational week 37 by C-section because of signs of fetal distress. She also presented with respiratory distress; short limbs were apparent, as was a cloverleaf skull deformity (Fig. 1 B); there was also anal atresia, for which a colostomy was performed in the first days of life. Imaging studies revealed the presence of multiple premature craniosynostoses, a malformation of the craniocervical junction with narrowing of the cervical canal and a thin cord, and the presence of multiple liver cysts. Clonic arm movements and nystagmus were interpreted as seizure equivalents, and developmental delay was ascertained. After multiple infections and seizures, the patient died at 7 mo of age. TREC and control genomic DNA were quantitated from the recovered newborn dried blood spots of P2 and a control infant born the same day; whereas both samples had detectable actin control copies (though lower than in samples stored desiccated at –20°C), TRECs were present in the control DNA but absent in DNA from P2.

The third patient (P3), a Hispanic female, was born at term by spontaneous vaginal delivery to a G5P3-4, with a birth weight of 2,405 g (less than third percentile). There was no known consanguinity, and the family history was negative for other affected relatives. She was ascertained after positive newborn screening for SCID (T cell excision circles, TRECs of 12/μL blood, with the normal range being >25/μL; control actin copy number was normal). In addition, she had marked skeletal dysplasia and developmental delay. Her facial features (Fig. 1 C) demonstrated hypotonia and long and up-slanting palpebral fissures, simple ears, and a small chin. She had wide-spaced nipples and a pectus excavatum, short limbs with extra skin folds at the shoulders and elbows, a severe thoracic scoliosis and lumbar lordosis,

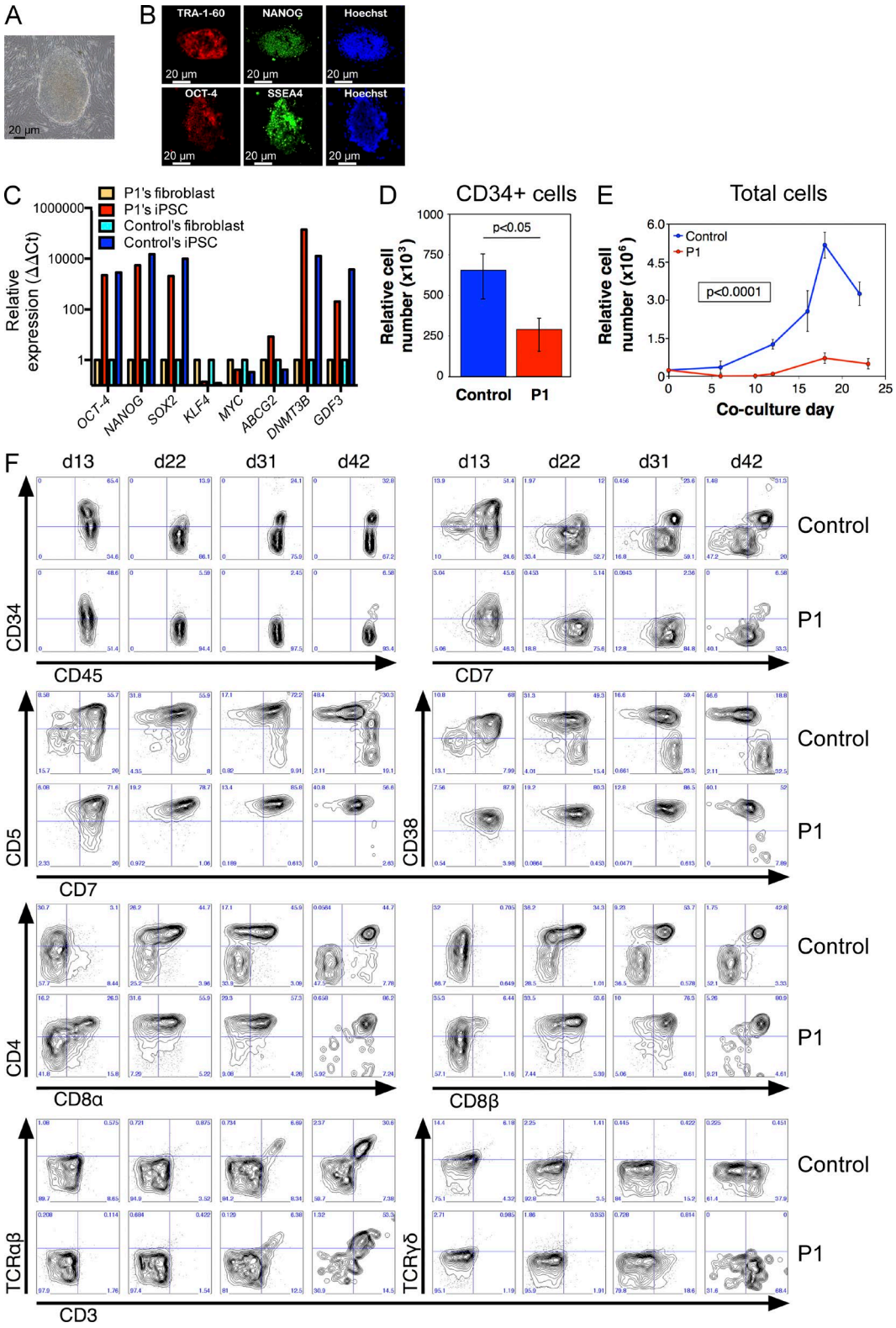

Figure 4. **Altered HPC expansion from EXTL3 R339W iPSCs.** (A and B) Morphological appearance (A) and immunofluorescence analysis (B) of P1's iPSCs. Shown are results for one representative iPSC clone of three that were tested. (C) Quantitative real-time PCR analysis of expression of pluripotency markers in patient and control iPSCs versus parental fibroblasts. Shown are results from one representative experiment of three. (D) Count of HPCs formed during embryoid body differentiation. Shown are mean values ± SEM from two independent experiments with three different iPSC clones for both control

a left single transverse crease, brachydactyly of the halluces and fifth toes, and two elbow dimples bilaterally. Her tone was markedly reduced, but there were no other neurological findings. In her first year of life, she had severe failure to thrive and required high calorie supplements and tube feedings with a G-tube. Metabolic assessment demonstrated hypertriglyceridemia. A magnetic resonance image of the brain and spine at 8 mo of age showed platyspondyly, lordoscoliosis, and pear-shaped vertebral ossification. No vertebral segmentation defects were identified. She had hypoplasia of the posterior C1 arch with narrowing of the cervical spinal canal and cord compression requiring neurosurgery. She was diagnosed with esotropia and chronic blepharitis with recurrent bilateral chalazion. Radiographs of the spine at 2 yr of age confirmed platyspondyly of the lower thoracic and lumbar spine with increased loss of vertebral height compared with disc spaces and progression of the thoracolumbar kyphosis to 90 degrees. A pelvic radiograph showed bilateral coxa vara, dysplastic changes of both hips, and subluxation of the left hip. When last examined at 2 yr and 5 mo of age, she was able to reach for objects, roll over, sit with support, and had several single words. Her height was 74 cm (−4.18 SD), her weight was 7.173 kg (−6.84 SD), and her head circumference was 46 cm (−1.87 SD). Spontaneous, partial improvement of immune function was observed at 1 yr and 4 mo of life. At that time, administration of intravenous immunoglobulins was suspended, and production of specific antibodies was observed in response to both killed/recombinant and live vaccines. At the time of last evaluation (2 yr and 7 mo), T cell counts were as follows: $CD3^+$, 1,317 cells/µl (normal values: 1,400–3,700); $CD4^+$, 817 cells/µl (of which 43% were naive; normal values: 53–86); and $CD8^+$, 545 cells/µl (of which 43.2% were naive; normal values 69–97). No evidence of somatic gene reversion was found upon high throughout sequencing of the *EXTL3* locus around position c.1382 in P3's T cell blasts.

Genetic analysis

All studies performed were approved by the institutional ethical review boards of Gaslini Children's Hospital, Boston Children's Hospital, and University of California, San Francisco. Informed consent was obtained from the patients' parents.

For P1 and P2, fragmented genomic DNA was purified with AMPure XP beads, and its quality was assessed with a Bioanalyzer (2100; Agilent Technologies). Sequencing libraries were generated using the SureSelect Human All Exon kit (v4; Agilent Technologies). The final libraries were quantified with a Qubit Fluorometer (Thermo Fisher Scientific), and the correct size distribution was validated on the Bioanalyzer (2100). Libraries were sequenced on a sequencing system (HiSeq 2000; Illumina) generating 100-bp paired-end reads. Raw reads were aligned onto the hg19 reference genome using NovoAlign (Novacraft Technologies). Data cleanup and variant calling were performed according to the Genome Analysis Toolkit Best Practices recommendations (Van der Auwera et al., 2013). Variant filtering was made with ANNOVAR (Wang et al., 2010) and with in-house *perl* and *bash* scripts, available upon request. Homozygosity mapping was achieved by the use of Homozygosity Mapper software (Seelow et al., 2009) on the merged *vcf* file of P1, P2, and parents. A comparison was made between the two affected siblings (cases) and the parents (controls) to detect region of autozygosity shared by the two affected siblings only. For P3, WES was performed at the University of California, Los Angeles Clinical Genomics Center, as described previously (Lee et al., 2014). Sanger sequencing was performed on genomic DNA extracted from fibroblasts (P1) or EBV-B cell lines (P2 and P3) using primer sequences and PCR conditions that are available upon request.

Western blot analysis of EXTL3 expression

Protein lysates were obtained from fibroblasts from a healthy control and P1, P1 cells complemented with a lentivirus (LV) vector expressing wild-type EXTL3 cDNA (P1 LV), and PBMCs from a healthy donor and P3, upon lysing cells in SDS sample buffer. Protein lysates were separated by 4–12% gradient SDS-PAGE, transferred onto nitrocellulose using an iBlot2 system (Thermo Fisher Scientific), and immunoblotted with anti-EXTL3 rabbit polyclonal antibody (Ab113063; Abcam) and anti–β-actin mAb (Cell Signaling Technology), followed by staining with secondary donkey anti–rabbit IgG HRP-conjugated antibody and HRP-conjugated sheep anti–mouse IgG (both from GE Healthcare). The blot was developed with SuperSignal West Femto substrate for EXTL3 and SuperSignal West Dura substrate for β-actin (both from Thermo Fisher Scientific). Bands were visualized using Omega Lum C Imager and software (Aplegen).

HS isolation, SDS-PAGE gradient, and disaccharide composition analysis

Proteoglycans were extracted from cell pellets by 7 M urea in PBS, pH 7.4, at 4°C with gentle stirring and isolated by diethylaminoethyl-Sepharose chromatography. To isolate HS, the total proteoglycan preparation was incubated with chondroitinase ABC (Seikagaku) followed by proteinase K, and samples were separated by diethylaminoethyl chromatog-

and P1. (E) Cell count of lymphoid precursors at different time points of OP9-DL4 T cell differentiation assay. Represented are means of two experiments from three different iPSC clones. Error bars represent SEM. (F) Normal surface expression of CD4 and CD8 molecules at late stages of OP9-DL4 T cell differentiation assay. Representative figures of two experiments from three different iPSC clones are shown. Statistical significance was assessed using two-tail unpaired Student's *t* test (D) or two-way ANOVA (E).

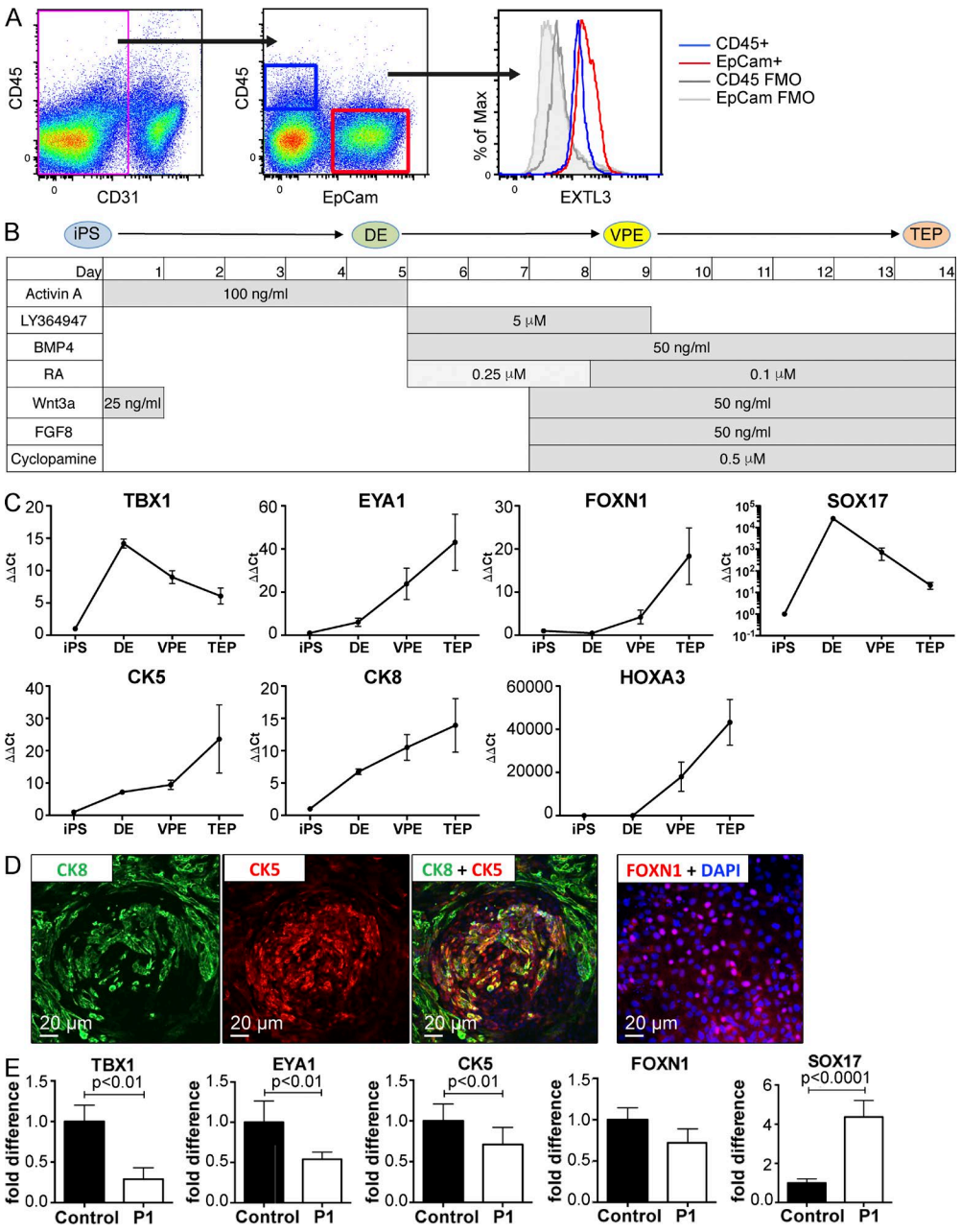

Figure 5. **Altered TEP cell differentiation from EXTL3-mutant iPSCs.** (A) Flow cytometric analysis of EXTL3 expression in total human thymic epithelial cell adhesion molecule (EpCam)$^+$ TECs and CD45$^+$ hematopoietic cells. FMO, fluorescence minus one. One representative experiment of two is shown. (B) Scheme of TEP differentiation protocol. (C) Gene expression profile during differentiation of control-derived iPSCs. (D) Immunofluorescence analysis of epithelial markers at TEP stage differentiation of control-derived iPSCs. (E) Differences in gene expression between control and P1 iPSC-derived TEPs. (C–E) Shown are representative results of at least three experiments, in each of which two different iPSC clones were tested for both P1 and healthy donor. Error bars represent SEM. iPS, iPSC; RA, retinoic acid; VPE, ventral pharyngeal endoderm. Statistical significance was assessed using two-tail unpaired Student's *t* test.

raphy. Bound materials were eluted by 2 M NaCl, dialyzed against autoclaved deionized water, and concentrated by lyophilization. The amount of HS was measured by the carbazole method (Bitter and Muir, 1962). 25 µg of the isolated HS were lyophilized, digested with heparinase I, II, and III, and then analyzed by extracted ion chromatogram liquid chromatography–mass spectrometry. To estimate the approximate size of total glycosaminoglycans and HS, 5 µg of each sample were fractionated by 5–12% gradient SDS-PAGE and visualized by Alcian blue staining.

Intracellular signaling in response to FGF-2 and cytokines

Fibroblasts from a healthy control, P1, and P1 LV fibroblasts were serum starved for 2 h and then stimulated in the presence or absence of 100 ng/ml human FGF-2 in DMEM. After 15 or 30 min, cells were lysed in SDS sample buffer. Protein lysates were separated by 5–15% gradient SDS-PAGE, transferred onto nitrocellulose membrane, and immunoblotted with rabbit anti-phospho ERK1/2 (Cell Signaling Technology) and HRP-conjugated donkey anti–rabbit IgG (BioLegend).

For the analysis of STAT5 phosphorylation in response to cytokines, PBMCs from two healthy controls and P3 were cultured in 96-well round-bottom plates (200,000 cells/well) in the presence of 10 ng/ml IL-2 or 10 ng/ml IL-7, in RPMI medium, 10% FBS, and APC-conjugated anti-CD4 mAb at 37°C and 5% CO_2 for 20 min. After washing, cells were permeabilized with Cytofix (BD) at 37°C for 10 min and then washed and stained with Pacific blue–conjugated anti-pSTAT5 (BD). The cells were washed, and pSTAT5 expression was analyzed by flow cytometry upon gating on live $CD4^+$ cells.

Analysis of EXTL3 expression in human thymus

Human thymus samples were collected from pediatric patients undergoing cardiac surgery (under the clinical protocol TIGET07, approved by the Ethical Committee of San Raffaele Scientific Institute). Thymic tissue was cleaned and minced into small pieces before digestion with Liberase/DNase I (Sigma-Aldrich). Digested tissue was depleted of CD45-positive cells using the AutoMACS Pro separator (Miltenyi Biotec) after incubation with anti–human CD45 microbeads (Miltenyi Biotec). After depletion, thymic cells were stained with antibodies anti–human CD45 APC, epithelial cell adhesion molecule/CD326 Pe-Vio770, HLA DR PE, CD31 APC-Vio770 (all from Miltenyi Biotec), and *Ulex europaeus* agglutinin I FITC (UEA I FITC; Vector Laboratories). After surface staining, thymic cells were fixed/permeabilized (Foxp3 Staining Buffer set; eBioscience) and stained intracellularly with anti-Extl3 antibody (Ab113063; Abcam), followed by a secondary goat anti–rabbit IgG Alexa Fluor 405 antibody (Invitrogen). Then, cells were acquired on a FACS Canto II cell analyzer (BD) and analyzed using FlowJo software (Tree Star).

Zebrafish studies

Zebrafish were maintained in accordance with Animal Research Guidelines at Boston Children's Hospital. The *extl3* (*box*^{tm70g}) and *ext2* (*dak*^{to273}) mutants and Tg(*rag2 :GFP*) transgenic zebrafish used in this study were previously described (Jessen et al., 2001; Lee et al., 2004).

For live imaging, zebrafish embryos were mounted in 0.8% low–melting point agarose or 4% methylcellulose containing 160 mg/L tricaine as previously described (Bertrand et al., 2010). Images were taken using a dissection stereoscopic microscope (Stereo Discovery V8; ZEISS) with a 0.63× objective and 8.3× optical zoom. To determine thymic volume, embryos were mounted in 0.8% low melting point agarose, and Z stacks of 25 sections every 2 µm, 512 × 512 pixels images (pixel size of 0.33 µm), were recorded using an upright microscope (C2si confocal NiE; Nikon) with a 25× objective. Image processing was done with NIS elements software (Nikon). Image post-processing and thymus isosurface analysis and quantification were done with Imaris software (Bitplane). Quantification of fin length in each fish was made by measuring the lengths of fin and eye in photographic images at a magnification of 8.3. For normalization, values were expressed as the ratio between lengths of fin to eye. For rescue experiments, full-length human *EXTL3* and *EXTL3* R339W cDNA were subcloned into the $pCS2^+$ expression vector. mRNA from both sequence-verified constructs was transcribed in vitro after NotI linearization, using the SP6 mMES SAGE mMACHINE kit (Ambion). For mRNA injections, 100 pg *EXTL3* or *EXTL3 R339W* mRNA was injected into the yolk of first–cell stage embryos. Embryos were analyzed for thymic volume or pectoral fin length at 6 d after fertilization and genotyped by PCR (primer sequences are available upon request), followed by EcoRV restriction digestion.

iPSC derivation, maintenance, and differentiation

Primary fibroblasts from P1 were reprogrammed to iPSCs by infection with a nonintegrating CytoTune Sendai viral vector kit (Thermo Fisher Scientific). Primary fibroblasts were plated in 12-well dishes at 50–80% confluency and transduced with the recombinant vectors according to the manufacturer's protocol. The medium was changed after 24 h of infection, and the cells were allowed to grow for 6 d. On day 7, the cells were replated onto γ-irradiated CF-1 mouse embryonic fibroblast (MEF) feeder cells (EMD Millipore) in DMEM/F12 medium containing 1% penicillin/streptomycin, 1% L-glutamine, 20% knockout serum replacement (KSR), 1% nonessential amino acids, and 100 µM β-mercaptoethanol (Thermo Fisher Scientific), supplemented with 10% MEF-conditioned medium (iPSC medium) on day 8, and the cells were cultured until colonies formed. iPSCs were selected based on morphology, subcloned for five to seven passages, manually picked as single-colony cells, seeded into wells of a 96-well plate containing 8.5 × 10^3 irradiated MEFs per well in standard human embryonic stem cell medium, and cultured at 37°C and 5% CO_2. Analysis of the stemness and pluripotency profile was performed by immunofluorescence and quantitative real-time PCR, as previously described (Rissone et al., 2015). For immunofluorescence staining, cells were washed with PBS, fixed at room temperature in 4% paraformaldehyde/PBS for 15 min, washed with PBS, permeabilized/blocked for 1 h at room temperature using 0.1% Triton X-100 in animal-free blocker (Vector Laboratories) followed by three PBS washes, then stained with fluorochrome-labeled antibodies against OCT-4, NANOG, SSEA4, and TRA-1-60, and counterstained with Hoechst 33342. Expression of stemness markers was assessed upon imaging with a Pathway 435 bioimager (BD) using a 10× lens. For quantitative real-time PCR, RNA

was extracted from 10^6 cells using the mirVana RNA isolation kit (Ambion) and reverse transcribed to cDNA with qScript cDNA supermix (Quanta Bioscience), according to the manufacturer's instructions. Expression of the *OCT4*, *NANOG*, *SOX2*, *KLF4*, *cMYC*, *ABCG2*, *DNMT3B*, and *GDF3* genes was quantified by real-time PCR with Power SYBR Green PCR master mix (Applied Biosystems) on a Real Time PCR analyzer (7500; Applied Biosystems) and normalized to the human β-actin (*hACTB*) gene expression using primers previously reported (Park et al., 2008). Relative expression compared with parental fibroblasts was calculated using the ΔΔCt method. Colonies with a robust stemness and pluripotency profile were assessed for karyotypic integrity by G-banding.

Embryoid body (EB) generation and CD34$^+$ cell isolation

Differentiation of iPSCs was performed in serum-free medium (StemPro-34; Thermo Fisher Scientific) containing 50 μg/ml L–ascorbic acid, 2 mM L-glutamine, 150 μg/ml transferrin, 0.45 μM monothioglycerol, and various cytokines and growth factors at 37°C, 5% O_2, and 5% CO_2, as previously described (Kennedy et al., 2012). iPSCs were feeder depleted on tissue-culture plates coated with Matrigel (BD) for 1 d. iPSC aggregates were transferred to ultra lo-attachment 6-well plates (Corning) containing cytokines, growth factors, and inhibitors for induction of differentiation toward definitive hematopoiesis. Cytokine and growth factor addition was as follows for embryoid body differentiation: days 0–3, 10 ng/ml BMP4; days 1–8, 10 ng/ml basic FGF; days 1.75–3, 5 μM SB-431542; days 4–8, 15 ng/ml vascular endothelial growth factor, 10 ng/ml IL-6, and 5 ng/ml IL-11; and day 6–8: 2 U/ml erythropoietin, 25 ng/ml IGF1, and 50 ng/ml stem cell factor.

After 8 d of differentiation, embryoid bodies were dissociated into single cells as previously described (Kennedy et al., 2012), stained with anti-CD34 PE-conjugated antibody (BD), followed by anti-PE–conjugated microbeads, and positively selected using a magnetic-activated cell-sorting (MACS) column (Miltenyi Biotec) as per the manufacturer's instructions. Cell yield and purity were assessed pre– and post–MACS purification by flow cytometry.

Co-culture with OP9-DL4 cells and in vitro T cell differentiation

OP9-DL4 cells were cultured in α-MEM containing 20% FBS (lot no. 1140803), 1% penicillin/streptomycin (Thermo Fisher Scientific), and phospho–ascorbic acid (Sigma-Aldrich) at 37°C and 5% CO_2. For co-culture, OP9-DL4 cells were plated in 6-well plates the previous day.

MACS-purified CD34$^+$ cells were counted and seeded at a density of 200,000–250,000 cells per well on a 6-well plate and differentiated toward the T cell lineage by co-culture with OP9-DL4 cells in OP9 medium containing 5 ng/ml recombinant human IL-7, 5 ng/ml recombinant human FLT3L, and 10 ng/ml recombinant human stem cell factor (Miltenyi Biotec) at 37°C and 5% CO_2, and T cell progenitors were passaged and co-cultured with fresh OP9-DL4 cells approximately every 5 d, as previously described (La Motte-Mohs et al., 2005).

At various time points during co-culture of iPSC-derived cells on OP9-DL4 stromal cells, analysis of the expression of T cell markers was performed. Cells were stained for 30 min on ice with combinations of the following mouse anti–human antibodies: CD3–Brilliant Violet 421, CD4–Alexa Fluor 700, CD8b-PE, CD31-FITC, CD34-PE, CD45RA-PE/CF594, TCRγδ-FITC (BD), CD5-PE/Cy7, CD7–Alexa Fluor 700, CD45-PC/eFluor780, TCRαβ-APC (eBioscience), CD8α-PE/Dazzle, and CD38–Brilliant Violet 421 (BioLegend). Cells were resuspended in flow cytometry buffer containing DAPI. Data were collected using an LSR Fortessa flow cytometer (BD) and analyzed using FlowJo (version 9.7.6).

Differentiation to TEP cells

Undifferentiated iPSCs were maintained on γ-irradiated MEFs and mechanically split by needle for passage. For differentiation, iPSCs were transferred to Corning Matrigel human epithelia stem cell–qualified Matrix-coated plates. After four to five passages, the cells were plated on the Matrigel-coated 24-well plates at a density of 2.5×10^5 cells/cm^2 and differentiated 24 h later. TEP differentiation protocol was based on a protocol by Parent et al. (2013) with minor modifications. During days 1–5 (d1–d5), differentiation was performed in RPMI 1640 media (Invitrogen) supplemented with 1% penicillin/streptomycin, 1% of L-glutamine, and increasing concentrations of KSR (0% on d1, 0.2% on d2–d3, and 2% on d4–d5). For d6–d14, cells were differentiated in DMEM/F12 with 1% penicillin/streptomycin, 1% L-glutamine, and 0.5% B-27 supplement (50×) serum-free medium (Thermo Fisher Scientific). The following factors were added: activin A, 100 ng/ml (d1–d5); Wnt3a, 25 ng/ml (d1) or 50 ng/ml (d8–d14); all-trans retinoic acid, 0.25 μM (d6–d8) or 0.1 μM (d9–d14); BMP4, 50 ng/ml (d6–d14); LY364947, 5 mM (d6–d9); FGF8b, 50 ng/ml (d8–d14); and KAAD-cyclopamine, 0.5 mM (d8–d14). Supplements and factors were from Invitrogen (B27 and KSR), R&D Systems (activin A, Wnt3a, BMP4, and FGF8b), Sigma-Aldrich (retinoic acid), and EMD Millipore (KAAD-cyclopamine and LY364947).

For the analysis of gene expression during differentiation of iPSCs to TEPs, at time points reported in Fig. 5 B, total RNA was isolated from by an RNeasy kit (QIAGEN), and cDNA was synthesized by a qScript cDNA Synthesis kit (Quanta Biosciences) according to the manufacturer's protocol. Real-time quantitative PCR was performed on a real-time PCR system (7500; Applied Biosystems) using PerfeCTa SYBR Green FastMix, Low ROX (Quanta Biosciences). After normalization to the housekeeping gene TATA-binding protein (TBP) gene *TBP*, for each sample, ΔΔCt values of gene expression were calculated relative to levels in undifferentiated control iPSCs.

Quantitative PCR primers for TBP, HOXA3, EYA1, and FOXN1 were as previously published (Parent et al., 2013).

Other primers were as follows: *SOX17* forward, 5′-GGC GCAGCAGAATCCAGA-3′ and reverse, 5′-CCACGACTT GCCCAGCAT-3′; *CK5* forward, 5′-TCTCGCCAGTCA AGTGTGTC-3′ and reverse, 5′-ATAGCCACCCACTCC ACAAG-3′; *CK8* forward, 5′-TCATCAAGAAGGATG TGGATG-3′ and reverse, 5′-ACCACAGATGTGTCCGAG AT-3′; and *TBX1* forward, 5′-ACGCCTTCCACAGCT CCT-3′ and reverse, 5′-CGCTATCTTTGCGTGGGTC-3′.

For confocal microscopy analysis, cells cultured in 24-well plates were fixed for 30 min in 4% paraformaldehyde with PBS at room temperature, washed twice in PBS, and then blocked for 1 h in 10% donkey serum and 0.1% Triton X with PBS at room temperature. Cells were incubated overnight at 4°C with the appropriate primary antibodies diluted in PBS and then incubated for 1 h at room temperature in the dark with secondary antibodies diluted in PBS. Nuclei were counterstained with DAPI. Images were taken with a spinning disk confocal microscope (UltraVIEW VoX; PerkinElmer).

The primary antibodies used were as follows: anti-CK5 (catalog no. ab24647; Abcam), anti-CK8 (catalog no. ab2530; Abcam), and rabbit anti-FOXN1 (catalog no. bs-6970R; Bioss). Secondary antibodies were Alexa Fluor 488–conjugated donkey anti–mouse IgG H and L (catalog no. ab150105; Abcam) and Alexa Fluor 594–conjugated donkey $F(ab')_2$ anti–rabbit IgG H and L (catalog no. ab150072; Abcam).

Online supplemental material

Fig. S1 shows a summary of the analysis of WES data in the affected patients and their respective parents. Tables S1 and S2 show the genetic variants compatible with causing disease in the two families analyzed.

ACKNOWLEDGMENTS

We thank Drs. Steven E. Brenner, Rajgopal Srinivasan, Uma Sunderam, and the UCLA Clinical Genomics Center Genomic Data Board for reviewing and interpreting WES data and Maurizio Fazio, Julie Perlin, and Anne Robertson for assistance with zebrafish experiments. The Cell Line and DNA Biobank from Patients Affected by Genetic Diseases (Istituto G. Gaslini; Telethon Network of Genetic Biobanks; project no. GTB12001) provided specimens.

This work was supported by the Intramural Research Program of the National Institute of Allergy and Infectious Diseases (NIAID), National Institutes of Health (NIH) and by a grant from NIAID, NIH (5R21AI113459 to L.D. Notarangelo), a grant from the Italian Ministry of Health (PE-2011-02347329 to S. Giliani and L.D. Notarangelo), a grant from the Swiss National Science Foundation (156260 to C. Rivolta), and a grant from the National Institute of Neurological Disorders and Stroke, NIH (R00NS083714 to F.E. Poulain). A. Superti-Furga is supported by the Faculté de Biologie et Medecine of the University of Lausanne. J.C. Zúñiga-Pflücker is supported by the Krembil Foundation and by a Canada Research Chair in Developmental Immunology.

The authors declare no competing financial interests.

Author contributions: A. Superti-Furga and L.D. Notarangelo directed the study. S. Volpi performed experiments and wrote the manuscript. Y. Yamazaki, P.M. Brauer, E. van Rooijen, A. Hayashida, H.S. Kuehn, I. Bortolomai, L. Du, K. Felgentreff, L.O. de Bruin, K. Hayashida, G. Freedman, G.E. Marcovecchio, K. Capuder, P. Rath, N. Luche, E.J. Hagedorn, S. Giliani, P.L. Poliani, L. Imberti, K. Dobbs, and H. Lee performed experiments. A. Slavotinek, M. Di Rocco, A. Buoncompagni, A. Martini, and J.M. Puck provided clinical and laboratory data on the patients. C. Rivolta, B. Royer-Bertrand, J. Manis, R.J. Linhardt, M. Bosticardo, S. Rosenzweig, J.C. Zúñiga-Pflücker, L. Zon, and P.W. Park supervised experiments. F.E. Poulain provided box and dak fish.

Submitted: 12 September 2016
Revised: 10 December 2016
Accepted: 10 January 2017

REFERENCES

Acquatella-Tran Van Ba, I., S. Marchal, F. François, M. Silhol, C. Lleres, B. Michel, Y. Benyamin, J.M. Verdier, F. Trousse, and A. Marcilhac. 2012. Regenerating islet-derived 1α (Reg-1α) protein is new neuronal secreted factor that stimulates neurite outgrowth via exostosin Tumor-like 3 (EXTL3) receptor. *J. Biol. Chem.* 287:4726–4739. http://dx.doi.org/10.1074/jbc.M111.260349

Anderson, G., and E.J. Jenkinson. 2001. Lymphostromal interactions in thymic development and function. *Nat. Rev. Immunol.* 1:31–40. http://dx.doi.org/10.1038/35095500

Bertrand, J.Y., N.C. Chi, B. Santoso, S. Teng, D.Y. Stainier, and D. Traver. 2010. Haematopoietic stem cells derive directly from aortic endothelium during development. *Nature.* 464:108–111. http://dx.doi.org/10.1038/nature08738

Bitter, T., and H.M. Muir. 1962. A modified uronic acid carbazole reaction. *Anal. Biochem.* 4:330–334. http://dx.doi.org/10.1016/0003-2697(62)90095-7

Bonafe, L., V. Cormier-Daire, C. Hall, R. Lachman, G. Mortier, S. Mundlos, G. Nishimura, L. Sangiorgi, R. Savarirayan, D. Sillence, et al. 2015. Nosology and classification of genetic skeletal disorders: 2015 revision. *Am. J. Med. Genet. A.* 167:2869–2892. http://dx.doi.org/10.1002/ajmg.a.37365

Borghesi, L.A., Y. Yamashita, and P.W. Kincade. 1999. Heparan sulfate proteoglycans mediate interleukin-7-dependent B lymphopoiesis. *Blood.* 93:140–148.

Brauer, P.M., I.M. Pessach, E. Clarke, J.H. Rowe, L. Ott de Bruin, Y.N. Lee, C. Dominguez-Brauer, A.M. Comeau, G. Awong, K. Felgentreff, et al. 2016. Modeling altered T-cell development with induced pluripotent stem cells from patients with *RAG1*-dependent immune deficiencies. *Blood.* 128:783–793. http://dx.doi.org/10.1182/blood-2015-10-676304

Busse, M., A. Feta, J. Presto, M. Wilén, M. Grønning, L. Kjellén, and M. Kusche-Gullberg. 2007. Contribution of EXT1, EXT2, and EXTL3 to heparan sulfate chain elongation. *J. Biol. Chem.* 282:32802–32810. http://dx.doi.org/10.1074/jbc.M703560200

Castriota-Scanderbeg, A., R. Mingarelli, G. Caramia, P. Osimani, R.S. Lachman, D.L. Rimoin, W.R. Wilcox, and B. Dallapiccola. 1997. Spondylo-mesomelic-acrodysplasia with joint dislocations and severe combined immunodeficiency: a newly recognised immuno-osseous dysplasia. *J. Med. Genet.* 34:854–856. http://dx.doi.org/10.1136/jmg.34.10.854

Clewing, J.M., H. Fryssira, D. Goodman, S.F. Smithson, E.A. Sloan, S. Lou, Y. Huang, K. Choi, T. Lücke, H. Alpay, et al. 2007. Schimke immunoosseous dysplasia: suggestions of genetic diversity. *Hum. Mutat.* 28:273–283. http://dx.doi.org/10.1002/humu.20432

Corder, W.T., M. Hummel, C. Miller, and N.W. Wilson. 1995. Association of kyphomelic dysplasia with severe combined immunodeficiency. *Am. J. Med. Genet.* 57:626–629. http://dx.doi.org/10.1002/ajmg.1320570422

Dooley, J., M. Erickson, W.J. Larochelle, G.O. Gillard, and A.G. Farr. 2007. FGFR2IIIb signaling regulates thymic epithelial differentiation. *Dev. Dyn.* 236:3459–3471. http://dx.doi.org/10.1002/dvdy.21364

El Masri, R., A. Seffouh, H. Lortat-Jacob, and R.R. Vivès. 2016. The "in and out" of glucosamine 6-*O*-sulfation: the 6th sense of heparan sulfate. *Glycoconj. J.* http://dx.doi.org/10.1007/s10719-016-9736-5

Esko, J.D., and U. Lindahl. 2001. Molecular diversity of heparan sulfate. *J. Clin. Invest.* 108:169–173. http://dx.doi.org/10.1172/JCI200113530

Gatti, R.A., N. Platt, H.H. Pomerance, R. Hong, L.O. Langer, H.E. Kay, and R.A. Good. 1969. Hereditary lymphopenic agammaglobulinemia associated with a distinctive form of short-limbed dwarfism and ectodermal dysplasia. *J. Pediatr.* 75:675–684. http://dx.doi.org/10.1016/S0022-3476(69)80465-8

Hockstein, N.G., D. McDonald-McGinn, E. Zackai, S. Bartlett, D.S. Huff, and I.N. Jacobs. 2004. Tracheal anomalies in Pfeiffer syndrome. *Arch. Otolaryngol. Head Neck Surg.* 130:1298–1302. http://dx.doi.org/10.1001/archotol.130.11.1298

Holley, R.J., C.E. Pickford, G. Rushton, G. Lacaud, J.T. Gallagher, V. Kouskoff, and C.L. Merry. 2011. Influencing hematopoietic differentiation of mouse embryonic stem cells using soluble heparin and heparan sulfate saccharides. *J. Biol. Chem.* 286:6241–6252. http://dx.doi.org/10.1074/jbc.M110.178483

Itan, Y., L. Shang, B. Boisson, M.J. Ciancanelli, J.G. Markle, R. Martinez-Barricarte, E. Scott, I. Shah, P.D. Stenson, J. Gleeson, et al. 2016. The mutation significance cutoff: gene-level thresholds for variant predictions. *Nat. Methods.* 13:109–110. http://dx.doi.org/10.1038/nmeth.3739

Jessen, J.R., T.N. Jessen, S.S. Vogel, and S. Lin. 2001. Concurrent expression of recombination activating genes 1 and 2 in zebrafish olfactory sensory neurons. *Genesis.* 29:156–162. http://dx.doi.org/10.1002/gene.1019

Kennedy, M., G. Awong, C.M. Sturgeon, A. Ditadi, R. LaMotte-Mohs, J.C. Zúñiga-Pflücker, and G. Keller. 2012. T lymphocyte potential marks the emergence of definitive hematopoietic progenitors in human pluripotent stem cell differentiation cultures. *Cell Reports.* 2:1722–1735. http://dx.doi.org/10.1016/j.celrep.2012.11.003

Kraushaar, D.C., S. Rai, E. Condac, A. Nairn, S. Zhang, Y. Yamaguchi, K. Moremen, S. Dalton, and L. Wang. 2012. Heparan sulfate facilitates FGF and BMP signaling to drive mesoderm differentiation of mouse embryonic stem cells. *J. Biol. Chem.* 287:22691–22700. http://dx.doi.org/10.1074/jbc.M112.368241

Lai, Y., D. Li, C. Li, B. Muehleisen, K.A. Radek, H.J. Park, Z. Jiang, Z. Li, H. Lei, Y. Quan, et al. 2012. The antimicrobial protein REG3A regulates keratinocyte proliferation and differentiation after skin injury. *Immunity.* 37:74–84. http://dx.doi.org/10.1016/j.immuni.2012.04.010

La Motte-Mohs, R.N., E. Herer, and J.C. Zúñiga-Pflücker. 2005. Induction of T-cell development from human cord blood hematopoietic stem cells by Delta-like 1 in vitro. *Blood.* 105:1431–1439. http://dx.doi.org/10.1182/blood-2004-04-1293

Langenau, D.M., A.A. Ferrando, D. Traver, J.L. Kutok, J.P. Hezel, J.P. Kanki, L.I. Zon, A.T. Look, and N.S. Trede. 2004. In vivo tracking of T cell development, ablation, and engraftment in transgenic zebrafish. *Proc. Natl. Acad. Sci. USA.* 101:7369–7374. http://dx.doi.org/10.1073/pnas.0402248101

Lee, H., J.L. Deignan, N. Dorrani, S.P. Strom, S. Kantarci, F. Quintero-Rivera, K. Das, T. Toy, B. Harry, M. Yourshaw, et al. 2014. Clinical exome sequencing for genetic identification of rare Mendelian disorders. *JAMA.* 312:1880–1887. http://dx.doi.org/10.1001/jama.2014.14604

Lee, J.S., S. von der Hardt, M.A. Rusch, S.E. Stringer, H.L. Stickney, W.S. Talbot, R. Geisler, C. Nüsslein-Volhard, S.B. Selleck, C.B. Chien, and H. Roehl. 2004. Axon sorting in the optic tract requires HSPG synthesis by ext2 (dackel) and extl3 (boxer). *Neuron.* 44:947–960. http://dx.doi.org/10.1016/j.neuron.2004.11.029

Levetan, C.S., L.V. Upham, S. Deng, L. Laury-Kleintop, V. Kery, R. Nolan, J. Quinlan, C. Torres, and R.J. El-Hajj. 2008. Discovery of a human peptide sequence signaling islet neogenesis. *Endocr. Pract.* 14:1075–1083. http://dx.doi.org/10.4158/EP.14.9.1075

MacDermot, K.D., R.M. Winter, J.S. Wigglesworth, and S. Strobel. 1991. Short stature/short limb skeletal dysplasia with severe combined immunodeficiency and bowing of the femora: report of two patients and review. *J. Med. Genet.* 28:10–17. http://dx.doi.org/10.1136/jmg.28.1.10

Matsumoto, Y., K. Matsumoto, F. Irie, J. Fukushi, W.B. Stallcup, and Y. Yamaguchi. 2010. Conditional ablation of the heparan sulfate-synthesizing enzyme Ext1 leads to dysregulation of bone morphogenic protein signaling and severe skeletal defects. *J. Biol. Chem.* 285:19227–19234. http://dx.doi.org/10.1074/jbc.M110.105338

McCormick, C., G. Duncan, K.T. Goutsos, and F. Tufaro. 2000. The putative tumor suppressors EXT1 and EXT2 form a stable complex that accumulates in the Golgi apparatus and catalyzes the synthesis of heparan sulfate. *Proc. Natl. Acad. Sci. USA.* 97:668–673. http://dx.doi.org/10.1073/pnas.97.2.668

Milne, C.D., S.A. Corfe, and C.J. Paige. 2008. Heparan sulfate and heparin enhance ERK phosphorylation and mediate preBCR-dependent events during B lymphopoiesis. *J. Immunol.* 180:2839–2847. http://dx.doi.org/10.4049/jimmunol.180.5.2839

Norton, W.H., J. Ledin, H. Grandel, and C.J. Neumann. 2005. HSPG synthesis by zebrafish Ext2 and Extl3 is required for Fgf10 signalling during limb development. *Development.* 132:4963–4973. http://dx.doi.org/10.1242/dev.02084

Ortmann, C., U. Pickhinke, S. Exner, S. Ohlig, R. Lawrence, H. Jboor, R. Dreier, and K. Grobe. 2015. Sonic hedgehog processing and release are regulated by glypican heparan sulfate proteoglycans. *J. Cell Sci.* 128:4462. http://dx.doi.org/10.1242/jcs.182360

Parent, A.V., H.A. Russ, I.S. Khan, T.N. LaFlam, T.C. Metzger, M.S. Anderson, and M. Hebrok. 2013. Generation of functional thymic epithelium from human embryonic stem cells that supports host T cell development. *Cell Stem Cell.* 13:219–229. http://dx.doi.org/10.1016/j.stem.2013.04.004

Park, I.H., R. Zhao, J.A. West, A. Yabuuchi, H. Huo, T.A. Ince, P.H. Lerou, M.W. Lensch, and G.Q. Daley. 2008. Reprogramming of human somatic cells to pluripotency with defined factors. *Nature.* 451:141–146. http://dx.doi.org/10.1038/nature06534

Picard, C., W. Al-Herz, A. Bousfiha, J.L. Casanova, T. Chatila, M.E. Conley, C. Cunningham-Rundles, A. Etzioni, S.M. Holland, C. Klein, et al. 2015. Primary immunodeficiency diseases: an update on the classification from the International Union of Immunological Societies Expert Committee for Primary Immunodeficiency 2015. *J. Clin. Immunol.* 35:696–726. http://dx.doi.org/10.1007/s10875-015-0201-1

Reichsman, F., L. Smith, and S. Cumberledge. 1996. Glycosaminoglycans can modulate extracellular localization of the wingless protein and promote signal transduction. *J. Cell Biol.* 135:819–827. http://dx.doi.org/10.1083/jcb.135.3.819

Revest, J.M., B. Spencer-Dene, K. Kerr, L. De Moerlooze, I. Rosewell, and C. Dickson. 2001a. Fibroblast growth factor receptor 2-IIIb acts upstream of *Shh* and *Fgf4* and is required for limb bud maintenance but not for the induction of *Fgf8*, *Fgf10*, *Msx1*, or *Bmp4*. *Dev. Biol.* 231:47–62. http://dx.doi.org/10.1006/dbio.2000.0144

Revest, J.M., R.K. Suniara, K. Kerr, J.J. Owen, and C. Dickson. 2001b. Development of the thymus requires signaling through the fibroblast growth factor receptor R2-IIIb. *J. Immunol.* 167:1954–1961. http://dx.doi.org/10.4049/jimmunol.167.4.1954

Rissone, A., K.G. Weinacht, G. la Marca, K. Bishop, E. Giocaliere, J. Jagadeesh, K. Felgentreff, K. Dobbs, W. Al-Herz, M. Jones, et al. 2015. Reticular dysgenesis-associated AK2 protects hematopoietic stem and progenitor cell development from oxidative stress. *J. Exp. Med.* 212:1185–1202. http://dx.doi.org/10.1084/jem.20141286

Rodewald, H.R. 2008. Thymus organogenesis. *Annu. Rev. Immunol.* 26:355–388. http://dx.doi.org/10.1146/annurev.immunol.26.021607.090408

Saldaña, J.I., A. Solanki, C.I. Lau, H. Sahni, S. Ross, A.L. Furmanski, M. Ono, G. Holländer, and T. Crompton. 2016. Sonic Hedgehog regulates thymic epithelial cell differentiation. *J. Autoimmun.* 68:86–97. http://dx.doi.org/10.1016/j.jaut.2015.12.004

Schilling, T.F., T. Piotrowski, H. Grandel, M. Brand, C.P. Heisenberg, Y.J. Jiang, D. Beuchle, M. Hammerschmidt, D.A. Kane, M.C. Mullins, et al. 1996. Jaw and branchial arch mutants in zebrafish I: branchial arches. *Development.* 123:329–344.

Schofer, O., I. Blaha, W. Mannhardt, F. Zepp, T. Stallmach, and J. Spranger. 1991. Omenn phenotype with short-limbed dwarfism. *J. Pediatr.* 118:86–89. http://dx.doi.org/10.1016/S0022-3476(05)81853-0

Seelow, D., M. Schuelke, F. Hildebrandt, and P. Nürnberg. 2009. HomozygosityMapper—an interactive approach to homozygosity mapping. *Nucleic Acids Res.* 37:W593–W599. http://dx.doi.org/10.1093/nar/gkp369

Senay, C., T. Lind, K. Muguruma, Y. Tone, H. Kitagawa, K. Sugahara, K. Lidholt, U. Lindahl, and M. Kusche-Gullberg. 2000. The EXT1/EXT2 tumor suppressors: catalytic activities and role in heparan sulfate biosynthesis. *EMBO Rep.* 1:282–286. http://dx.doi.org/10.1093/embo-reports/kvd045

Stewart, M.D., and R.D. Sanderson. 2014. Heparan sulfate in the nucleus and its control of cellular functions. *Matrix Biol.* 35:56–59. http://dx.doi.org/10.1016/j.matbio.2013.10.009

Su, M., R. Hu, J. Jin, Y. Yan, Y. Song, R. Sullivan, and L. Lai. 2015. Efficient in vitro generation of functional thymic epithelial progenitors from human embryonic stem cells. *Sci. Rep.* 5:9882. http://dx.doi.org/10.1038/srep09882

Sugaya, N., H. Habuchi, N. Nagai, S. Ashikari-Hada, and K. Kimata. 2008. 6-*O*-sulfation of heparan sulfate differentially regulates various fibroblast growth factor-dependent signalings in culture. *J. Biol. Chem.* 283:10366–10376. http://dx.doi.org/10.1074/jbc.M705948200

Sun, X., J. Xu, H. Lu, W. Liu, Z. Miao, X. Sui, H. Liu, L. Su, W. Du, Q. He, et al. 2013. Directed differentiation of human embryonic stem cells into thymic epithelial progenitor-like cells reconstitutes the thymic microenvironment in vivo. *Cell Stem Cell.* 13:230–236. http://dx.doi.org/10.1016/j.stem.2013.06.014

Tavormina, P.L., R. Shiang, L.M. Thompson, Y.Z. Zhu, D.J. Wilkin, R.S. Lachman, W.R. Wilcox, D.L. Rimoin, D.H. Cohn, and J.J. Wasmuth. 1995. Thanatophoric dysplasia (types I and II) caused by distinct mutations in fibroblast growth factor receptor 3. *Nat. Genet.* 9:321–328. http://dx.doi.org/10.1038/ng0395-321

Van der Auwera, G.A., M.O. Carneiro, C. Hartl, R. Poplin, G. Del Angel, A. Levy-Moonshine, T. Jordan, K. Shakir, D. Roazen, J. Thibault, et al. 2013. From FastQ data to high confidence variant calls: the Genome Analysis Toolkit best practices pipeline. *Curr. Protoc. Bioinformatics.* 43:11.10.1–11.10.33. http://dx.doi.org/10.1002/0471250953.bi1110s43

van Eeden, F.J., M. Granato, U. Schach, M. Brand, M. Furutani-Seiki, P. Haffter, M. Hammerschmidt, C.P. Heisenberg, Y.J. Jiang, D.A. Kane, et al. 1996. Genetic analysis of fin formation in the zebrafish, Danio rerio. *Development.* 123:255–262.

Wang, K., M. Li, and H. Hakonarson. 2010. ANNOVAR: functional annotation of genetic variants from high-throughput sequencing data. *Nucleic Acids Res.* 38:e164. http://dx.doi.org/10.1093/nar/gkq603

Wrenshall, L.E., J.L. Platt, E.T. Stevens, T.N. Wight, and J.D. Miller. 2003. Propagation and control of T cell responses by heparan sulfate-bound IL-2. *J. Immunol.* 170:5470–5474. http://dx.doi.org/10.4049/jimmunol.170.11.5470